Journal of
Materials Chemistry C

Accepted Manuscript

ROYAL SOCIETY OF CHEMISTRY

rsc.li/materials-c

View Article Online
DOI: 10.1039/C8TC00628H

ROYAL SOCIETY OF CHEMISTRY View Article Online
DOI: 10.1039/C8TC00628H

Journal Name

ARTICLE

Structure Engineering: Extending the Length of Azaacene Derivatives through Quinone Bridge

Received 00th January 20xx,
Accepted 00th January 20xx

DOI: 10.1039/x0xx00000x

www.rsc.org/

Zilong Wang,‡[a] Zongrui Wang,‡[a] Yecheng Zhou,[b] Peiyang Gu,[a] Guangfeng Liu,[a] Kexiang Zhao,[a] Lina Nie,[a] Qingsheng Zeng,[a] Jing Zhang,[a] Yongxin Li,[c] Rakesh Ganguly,[c] Naoki Aratani,[d] Li Huang,[b] Zheng Liu,[a] Hiroko Yamada,*[d] Wenping Hu,*[e] and Qichun Zhang*[ac]

Increasing the length of azaacene derivatives through quinone bridges is very important because these materials could have deep LUMO energy levels and larger overlapping in the solid state, which would have great applications in organic semiconducting devices. Here, two fully characterized large quinone-fused azaacenes **Hex-CO** and **Hept-CO** prepared through a novel palladium-catalyzed coupling reaction are reported. Our research clearly proved that the quinone unit can be employed as the bridge to extend the molecular conjugation length, increase the molecular overlapping, and engineer the molecular stacking mode. **Hex-CO** shows lamellar 2-D π-stacking modes, while **Hept-CO** shows 1-D π-stacking and adopts 3-D interlocked stacking mode with the adjacent molecular layers vertical to each other. With the deep LUMO energy levels (~ -4.27 eV), **Hex-CO** and **Hept-CO** were both demonstrated as electron-transport layers. Their charge transport property has been investigated through OFETs and theoretical calculations. Due to the different stacking modes, **Hex-CO** shows a higher electron mobility of 0.22 $cm^2 V^{-1} s^{-1}$ than **Hept-CO** (7.5×10^{-3} $cm^2 V^{-1} s^{-1}$) in the single-crystal-based OFET. Our results provide a new route on the structure engineering through extending the azaacene derivatives by quinone bridge, which can be profound in organic electronics.

Introduction

Engineering the stacking structures and molecular orbital energy levels to improve the charge transport has a profound significance in organic electronics. Azaacene derivatives, an important class of polycyclic aromatic hydrocarbons, has been demonstrated as n-type and ambipolar semiconductors in many applications including organic light-emitting diodes[1], organic memory devices[2], photoelectrochemical cells[3], solar cells[4], and especially in organic field effect transistors (OFETs).[5] Since stacking modes and molecular orbital energy levels are two key factors to affect the performance of organic electronic devices, it is crucial to manage them through molecular engineering. Generally, extending the conjugation of azaacenes is a good strategy to improve their performance because such approaching can efficiently increase π-π interactions, change molecular stacking modes in the solid state, and shift the molecular orbital energy levels concurrently.[6] This extension can be realized by several methods[7] such as Diels–Alder reactions, condensation reactions, and palladium-catalyzed way. However, employing quinone as a building unit to extend the length of azaacene derivatives and reduce their LUMO energy levels is rarely cultured.[8] Such gap strongly encourages us to investigate this type of materials and find their practical applications.

In fact, in the arena of acenes, quinones have been widely employed as intermediates to construct oligoacenes through nucleophilic substitution reactions[9] with TIPS-alkynyllithium[10] or phenyllithium,[11] followed by reduction, or through directly reducing the quinones into benzene rings.[12] Such a strategy should be also promising to build larger azaacenes or quinone-fused azaacenes. Normally, quinone units can be introduced into the backbone of azaacene derivatives through Diels–Alder reactions,[13] condensation reactions between cyclohexanehexone and diamine compounds,[14] and direct oxidization of azaacenes.[15] However, all of these methods have some disadvantages: either the limited choices of reactants or the harsh oxidation conditions. To address these issues, we here reported a new method (namely, palladium-catalyzed reaction) to prepare quinone-embedded large azaacene derivatives. Two novel quinone-embedded large azaacene derivatives **Hex-CO** and **Hept-CO** with six and seven six-membered rings fused in one row are synthesized through this method. The stacking

[a] School of Materials Science and Engineering, Nanyang Technological University Singapore, Singapore 639798, Singapore. *E-mail: qczhang@ntu.edu.sg
[b] Department of Physics, South University of Science and Technology of China, Shenzhen 518055, China
[c] Division of Chemistry and Biological Chemistry, School of Physical and Mathematical Sciences, Nanyang Technological University, Singapore 639798, Singapore
[d] Graduate School of Materials Science, Nara Institute of Science and Technology, Ikoma 630-0192, Japan. *E-mail: hyamada@ms.naist.jp
[e] Tianjin Key Laboratory of Molecular Optoelectronic Sciences, Department of Chemistry, School of Science & Collaborative Innovation Center of Chemical Science and Engineering (Tianjin), Tianjin University, Tianjin 300072, China. *E-mail: huwp@tju.edu.cn

†Electronic Supplementary Information (ESI) available: [Crystallographic data in CIF and experimental methods and instruments, synthesis details, ^{1}H NMR, ^{13}C NMR, HR-MS, molecular crystal structures, AFM images, micro crystals images, theoretical calculations details of charge transfer in PDF]. See DOI: 10.1039/x0xx00000x

‡ The two authors contribute equally to this paper.

View Article Online
DOI: 10.1039/C8TC00628H

modes of azaacene derivatives can be engineered by adjusting the conjugation length through the quinone bridge. Hence, though **Hept-CO** with 1-D π-stacking mode in the crystal does not show very high mobility in the OFET devices, **Hex-CO** does exhibit much better electron-transporting ability due to the engineered 2-D π-stacking mode.

Results and Discussion

Synthesis

The synthetic route to prepare **Hex-CO** and **Hept-CO** is shown in Scheme 1. Compounds **1**[16], **2**[17] and **4**[17] were synthesized according to the reported procedures. The active dichloride quinone compounds **2** and **3** can react with the diamine compound **1** through double Buchwald–Hartwig reactions giving **5** (74%) and **6** (85%) in good yields. After oxidizing **5** and **6** with active MnO_2, the target compounds **Hept-CO** and **Hex-CO** can be obtained. Note that the same reaction between **1** and **4** did not produce **7**, instead, **8** was obtained, which might be due to the high reactivity of the ketone in **4.** Since compound **8** is not the target molecule, it will not be further discussed in the following part. The as-prepared new compounds were confirmed by ^{1}H NMR, ^{13}C NMR, HR-MS and single crystal X-ray diffraction (Fig. S1-Fig. S15).

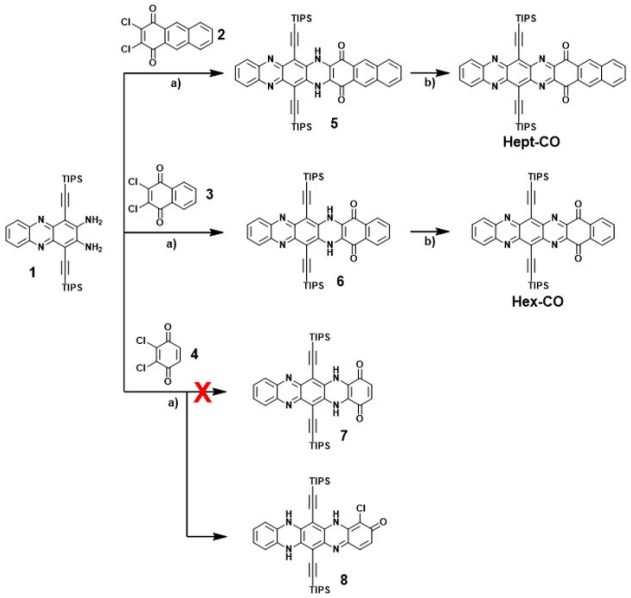

Scheme 1. Synthetic route of **Hept-CO** and **Hex-CO**. Conditions: (a) $CHCl_3$, Hünig's base, $Pd_2(dba)_3$, AcOH, RuPhos, 70 °C, 48 h; (b) MnO_2, CH_2Cl_2, RT.

Single-crystal X-ray structure

The flake-like black crystals of **Hept-CO** were obtained by placing a chlorobenzene solution in methanol atmosphere for about one week. These crystals are good enough for single-crystal X-ray diffraction analysis. Fig. 1a and 1b show that **Hept-CO** has a planar backbone. The molecular stacking structures (Fig. 1c–1e) indicate that **Hept-CO** molecules form dimers firstly (marked with green color in Fig. 2c and 2d) through a strong π-π interaction with a mean short distance of 3.275 Å. Then, these 1-D π-stacking stripes are constructed by these dimers through mild π-π interactions (3.396 Å, Fig. 1c and 1d). Subsequently, these 1-D stripes aggregate themselves together by C-H-π interactions to form 2-D layers (Fig. 1d). Finally, a 3-D stacking structure was built by the interlocking of adjacent 2-D layers (Fig. 1e and 1f), in which the adjacent molecular layers are vertical to each other. This interlocked 3-D stacking arrangement deviates the packing pattern of **Hept-CO** from the ideal lamellar 2-D π-stacking mode, which will hinder the effective charge transport to a considerable extent.

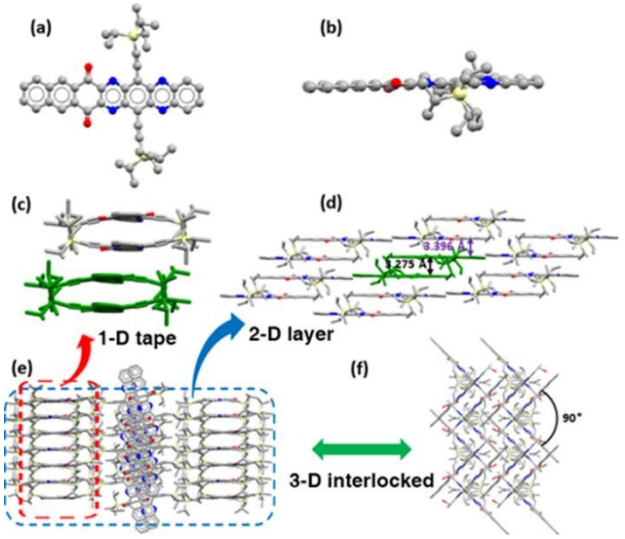

Fig. 1. Single-crystal X-ray structure of **Hept-CO** (Hydrogen and solvent molecules (MeOH) are removed for clarification): (a) top view and (b) side view of the molecule configuration (color scheme: C, gray; N, blue; Si, yellow; O, red); (c) 1-D molecular stacking structure: side view along the long axis of the conjugation backbone; (d) 2-D molecular stacking layer: side view perpendicular to long axis of the conjugation backbone; (one dimer is shown in green color); (e) and (f): the final 3-D molecular interlocked stacking structure.

The rod-like single crystals of **Hex-CO** were obtained by placing a chloroform solution in methanol atmosphere for about three days. In the structure of **Hex-CO**, the backbone possesses a planar configuration (Fig. 2a and 2b). The molecular stacking modes also indicate that **Hex-CO** molecules form dimers firstly (marked with green color in Fig. 2c and 2d) through a strong π-π interaction with a mean short distance of 3.310Å, which is larger than that of **Hept-CO**. This suggests that the neighboring molecules tend to form dimers. The asymmetry and the strong π-π interactions caused by the extended conjugations promote the formation of the dimers. Subsequently, these dimers stack together by adopting a lamellar 2-D π-stacking motif, which is an ideal packing mode for high-performance OFETs.[18] The mean short distances between these dimers are 3.342 Å and 3.371 Å (Fig. 2c), which indicates the existence of strong π-π interactions. These factors strongly suggest that **Hex-CO** should be a suitable candidate for OFET devices.

Comparing the molecular packing modes between **Hex-CO** and **Hept-CO**, it can be easily concluded that adjusting the length of the azaacene derivatives through the quinone bridge is a practical tool to engineer the molecule packing structure in the solid state.

View Article Online
DOI: 10.1039/C8TC00628H

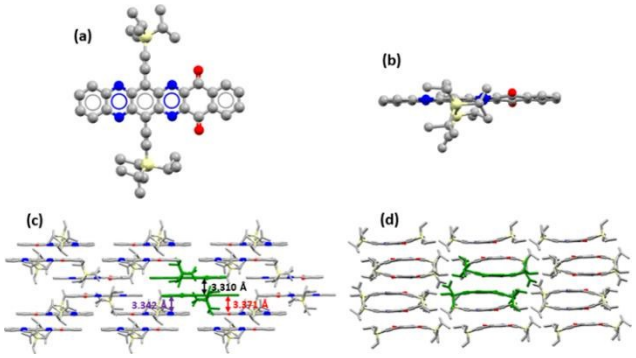

Fig. 2. Single-crystal X-ray structure of **Hex-CO**: (a) Top view and (b) side view of the molecule configuration (color scheme: C, gray; N, blue; Si, yellow; O, red. The CH_3OH solution molecules and H atoms are omitted for clarity); Molecular stacking structures (one dimer is shown in green color): (c) side view perpendicular to long axis of the conjugation backbone and (d) side view along the long axis of the conjugation backbone.

Molecular orbital energy levels

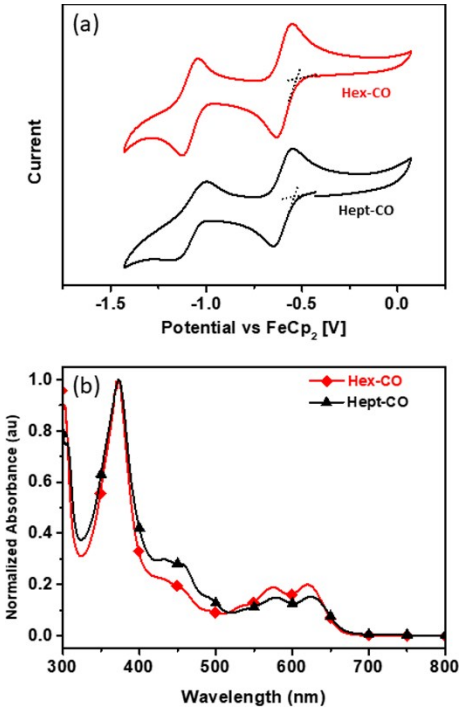

Fig. 3. (a) Cyclic voltammetry curves of **Hex-CO** and **Hept-CO** (Electrolyte: 0.1M nBu_4NPF_6, Scanning speed: 50 mV/s); (b) UV-vis absorption spectra of **Hex-CO** and **Hept-CO** in CH_2Cl_2. Concentration: 10^{-5} M, room temperature.

The LUMO energy levels and optical band gaps of **Hex-CO** and **Hept-CO** were studied by cyclic voltammetry (CV) and UV-vis absorption (UV), respectively. As shown in Fig. 3a, the CV curves of **Hex-CO** and **Hept-CO** are same to each other with the onset potentials of -0.53V and -1.03V for **Hex-CO**; and -0.54V and -1.04V for **Hept-CO**. The calculated LUMO and LUMO+1 energy levels from these data are -4.27 eV and -3.96 eV for **Hex-CO**; -4.26 eV and -3.97 eV for **Hept-CO**. The deep LUMO energy levels suggest that these materials are good n-type semiconductor candidates. The UV-vis absorption spectra of **Hex-CO** and **Hept-CO** are also similar to each other as shown in Fig. 3, where three absorption peaks between 400 nm and 700 nm are found. Their onset absorptions at 666 nm for **Hex-CO** and 668 nm for **Hept-CO** suggest that their optical band gaps are around 1.86 eV. This value is similar to that of the reported TIPS-azapentacenes,[19] which suggests that the aromaticity breaks at quinone units. According to the optical band gaps and LUMO energy values, the HOMO energies can be calculated to be -6.13 eV for **Hex-CO** and -6.12 eV for **Hept-CO**.

The frontier molecular orbitals are theoretically investigated by quantum chemistry calculations performed with the Gaussian09 package using density functional theory (DFT) calculation at the B3PW91/6-31G(d) level as shown in Fig. 4.[20] The electron distributions in HOMOs of **Hex-CO** and **Hept-CO** are mainly delocalized on the azatetraacene parts. Although electron distributions in LUMOs are delocalized on the azatetraacenes species and the quinone units, they cannot pass through the quinone bridges to the other side. This suggests that quinone units have a significant contribution in lowering the LUMO levels of azaacene derivatives while the extended lengths on the other side of quinone bridges almost have no contribution to molecular orbital energy levels. This conclusion can be supported by the results of the photophysical study and electrochemical experiments (Table 1).

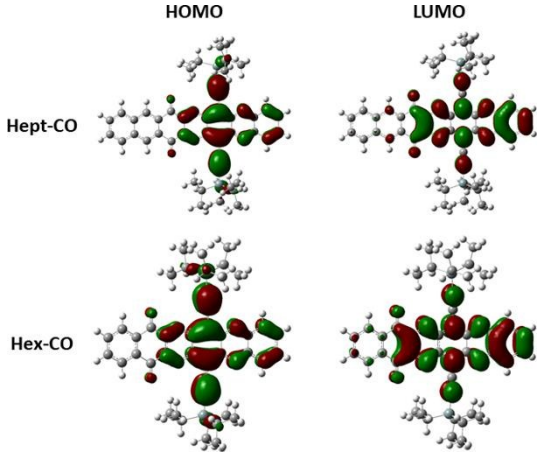

Fig. 4. The electron density distribution of HOMOs and LUMOs of **Hex-CO** and **Hept-CO** by DFT calculation.

Table 1. Photophysical, electrochemical, DFT calculation data and energy levels of **Hex-CO** and **Hept-CO**.

Compd.	$E_{onset, red}^{1}$ (V)	$E_{onset, red}^{2}$ (V)	$E_{HOMO, DFT}$ (eV)	$E_{HOMO, opt}$ (eV)	$\lambda_{onset, abs}$ (nm)
Hex-CO	-0.53	-1.03	-5.65	-6.13	666
Hept-CO	-0.54	-1.04	-5.60	-6.12	668
	$E_{LUMO, CV}$ (eV)	$E_{LUMO+1, CV}$ (eV)	$E_{LUMO, DFT}$ (eV)	Gap_{DFT} (eV)	Gap_{opt} (eV)
Hex-CO	-4.27	-3.96	-3.64	2.01	1.86
Hept-CO	-4.26	-3.97	-3.60	2.00	1.86

View Article Online
DOI: 10.1039/C8TC00628H

Charge transport behavior

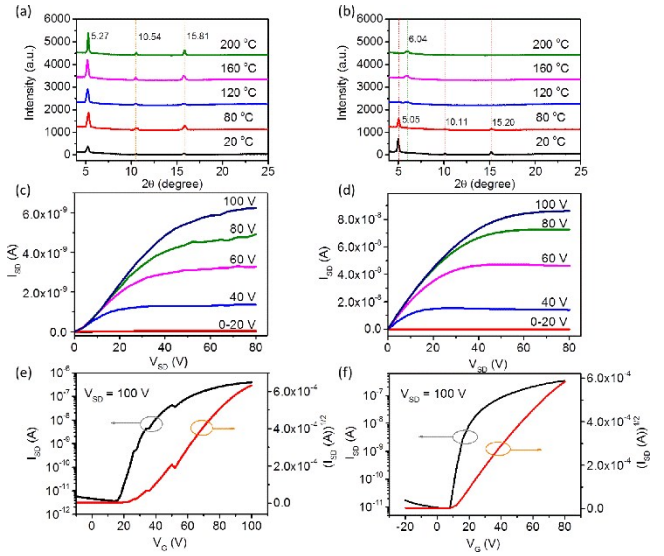

Fig. 5. X-ray diffraction patterns of spin-coating thin films of (a) **Hex-CO** and (b) **Hept-CO** at different annealing temperatures; (c, d) Representative output and (e, f) transfer characteristics of organic thin-film field effect transistors based on **Hex-CO** (c, e) and **Hept-CO** (d, f) at their optimized temperature (**Hex-CO**, 80 °C; **Hept-CO**, 80 °C).

Table 2. The electrical properties of the thin-film OFET based on **Hex-CO** and **Hept-CO** at different annealing temperatures.

Compd.	$T_{annealing}$ (°C)	μ (in 10^{-3} $cm^2V^{-1}s^{-1}$) [a]	V_T (V)	I_{on}/I_{off}
Hex-CO	30	2.3 (3.8)	44.6	10^4
	80	2.3 (2.8)	23.1	10^4
	120	0.24 (0.35)	18.0	10^3
Hept-CO	30	2.3 (2.8)	21.4	10^4
	80	5.5 (9.3)	21.5	10^5
	120	2.0 (2.3)	7.68	10^4
	160	1.8 (2.3)	22.1	10^4
	200	1.1 (1.5)	11.7	10^4

[a] Maximum mobility values (in brackets) and the average values of more than 5 devices measured in vacuum.

To investigate the charge transport behaviors of **Hex-CO** and **Hept-CO**, the bottom-gate top-contact (BGTC) organic field effect transistors (OFETs) have been fabricated with *n*-octadecyltrimethoxylsilane (OTS)-modified SiO_2 (300 nm, C_i = 11 nF cm^{-2}) as the dielectric layer, highly n-doped silicon wafer as the gate electrode, and gold as source/drain electrodes. Firstly, we investigated the charge transport in spin-coated thin films w/o annealing. The key parameters of thin-film OFETs have been summarized in **Table 2**, from where, we can conclude that without annealing their thin-film devices exhibit a slightly different electron charge transport with the best electron mobilities of 3.8 × 10^{-3} cm^2 V^{-1} s^{-1} for **Hex-CO** and 9.3 × 10^{-3} cm^2 V^{-1} s^{-1} for **Hept-CO** (Fig. 5), although these two compounds own different single crystal structures. The slightly higher performance of **Hept-CO** might ascribe to its more continuous films than that of **Hex-CO**, which can be evidenced from the results of X-ray diffraction and AFM (Fig. 5 and Fig. S17). With annealing, the loss of the effective charge transport path (or the loss of the mobility) for **Hex-CO** can be observed, which can be due to the discontinuous films caused by the molecular aggregation. As to the film of **Hept-CO**, the morphology exhibits a distinct change from granular grains to the clustered nanorods when the temperature goes up to 120 °C, and correspondingly, the XRD also shows an apparent peak shift from 5.18° to 6.02°, indicating a phase change happens, which disturbs the efficient charge transport and leads to the reduced performance.

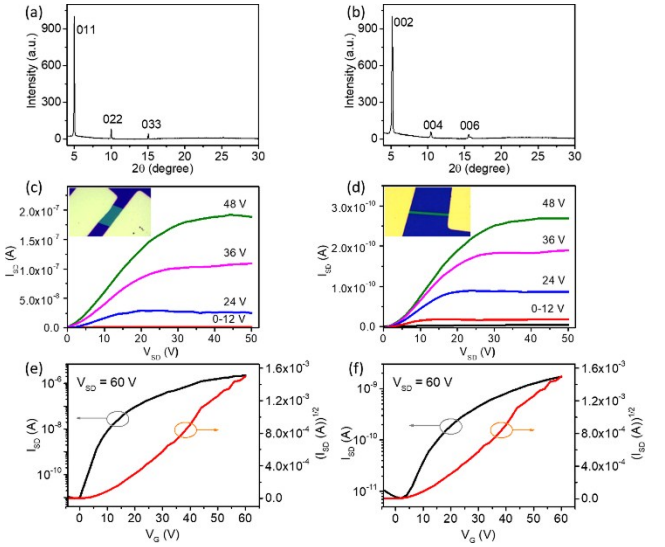

Fig. 6. X-ray diffraction patterns of as-casted micro crystal (a) **Hex-CO** and (b) **Hept-CO**; (c, d) Representative output and (e, f) transfer characteristics of organic single-crystal field effect transistors based on **Hex-CO** (c, e) and **Hept-CO** (d, f). Inset of (c, d) is the correspondingly typical device setup.

Single-crystal based FETs of **Hex-CO** and **Hept-CO** were also fabricated to investigate their intrinsic charge transports.[21] Through a drop-casting method, micro/nanometer-sized crystals suitable for device fabrication were obtained (Fig. S18: **Hex-CO**, sheet; **Hept-CO**, ribbon). The strong and sharp X-ray diffraction peaks (Fig. 6a and 6b) indicate the high quality of the as-prepared crystals, where the microcrystals of **Hex-CO** were parallel to the substrate with the (011) lattice plane while the microcrystals of **Hept-CO** employed their (001) lattice plane. The bottom-contact single-crystal OFETs based on these microcrystals have fabricated using stripped gold films as source/drain electrodes to avoid the heat emission damage on the crystals.[22] All these devices exhibit typical n-type behaviors and Fig. 6 shows the typical output and transfer characteristics. Based on these transfer curves, **Hex-CO** exhibits the best electron mobility up to 0.22 cm^2 V^{-1} s^{-1}, which is almost two magnitudes higher than that in thin film. In comparison, **Hept-CO** exhibits the similar electron mobility (7.5 × 10^{-3} cm^2 V^{-1} s^{-1}) to that of its thin film. The apparently better performance of **Hex-CO** over **Hept-CO** could be ascribed to the different molecular stacking modes that the dimers of **Hex-CO** show a lamellar 2-D π-stacking mode while the dimers of **Hept-CO** shows 1-D π-stacking and adopts 3-D interlocked stacking mode with the adjacent molecular layers vertical to each other. The

View Article Online
DOI: 10.1039/C8TC00628H

latter factor could partly hinder the efficient charge transport since the electrons are confined in one-dimensional channels.[23]

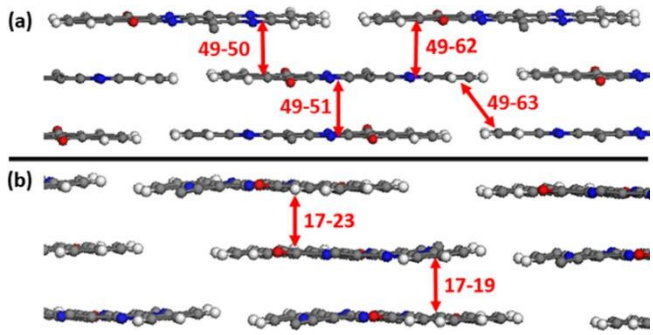

Fig 7. Hoping route of (a) **Hex-CO** and (b) **Hept-CO** in the crystal (the hydrogen atoms are omitted for clarification); The intermolecular electronic couplings of hole transfer (V_h) and electron transfer (V_e) for the center molecule (a) **49** and (b) **17** are calculated at DFT/B3LYP/6-31G(d) level, which were obtained through a direct evaluation of the coupling element between frontier orbitals using the unperturbed density matrix of the dimer Fock operator.[26]

Table 3. The electronic couplings for the hopping pathways of Hex-CO and Hept-CO.

Compd.	Pathway	center-center/Å	Vh/meV	Ve/meV
Hex-CO	**49-50**	9.59	8.03	33.10
	49-51	6.42	1.24	64.91
	49-62	9.20	23.63	61.71
	49-63	15.20	0.08	13.71
Hept-CO	**17-19**	5.62	51.62	96.54
	17-23	8.68	-22.30	-51.14

To further understand how the molecular structures affect their OFET performance, theoretical calculations based on single-crystal structures with the Marcus electron transfer theory and an incoherent random walk model have been carried out to evaluate hole and electron mobilities.[24] The reorganization energies of hole and electron were calculated to be 240.0 meV and 222.9 meV for **Hex-CO** and 243.8 meV and 212.0 meV for **Hept-CO**, respectively, at the DFT/B3LYP/6-31G(d) level. The transfer integrals were also calculated as shown in Fig. 7, Fig. S19, and Fig. S20, as well as summarized in Table 3, Table S2, and Table S3. Very large electron transfer integrals can be observed inside the dimers (64.91 meV for **Hex-CO** and 96.54 meV for **Hept-CO**), The electron transfer integrals between the dimers in the π-π stacking directions are also very large (61.71 meV and 33.10 meV for **Hex-CO**, and -51.14 meV for **Hept-CO**), which are similar and even higher than that of the classic n-type semiconductor 5,7,12,14-tetraazapentacene (TIPS-TAP) (-57.12 meV).[25] These large transfer integrals are coincident with the strong π-π interactions caused by the large conjugation of **Hept-CO** and **Hex-CO**. For the comparison of **Hex-CO** and **Hept-CO**, although they both have large electron transfer integrals, the lamellar 2-D π-stacking mode of **Hex-CO** dimers make it more beneficial for the efficient charge transport than **Hept-CO**, resulting in a higher electron mobility of **Hex-CO**.

Conclusions

Two new quinone-embedded large azaacene derivatives **Hex-CO** and **Hept-CO** have been synthesized in good yields through palladium-catalyzed coupling reactions. The single crystal structure analysis indicates that **Hex-CO** shows lamellar 2-D π-stacking modes while **Hept-CO** shows 1-D π-stacking and adopts 3-D interlocked stacking mode with the adjacent molecular layers vertical to each other. The quinone units offer **Hex-CO** and **Hept-CO** deep LUMO energy levels of -4.27 eV and -4.26 eV, respectively. The theoretical study shows that the electron reorganization energy of **Hex-CO** and **Hept-CO** are calculated to be 222.9 meV and 212.0 meV, respectively. **Hex-CO** and **Hept-CO** have very high largest transfer integrals for electron transport: 61.71 meV for **Hex-CO** and -51.14 meV for **Hept-CO** respectively, excluding that inside the dimers (64.91 meV for **Hex-CO** and 96.54 meV for **Hept-CO**), which might benefit for electron transport. The thin-film OFET devices based on **Hex-CO** and **Hept-CO** show the best electron mobilities up to 3.8×10^{-3} cm^2 V^{-1} s^{-1} and 9.3×10^{-3} cm^2 V^{-1} s^{-1}, respectively, while the devices based on their single crystals exhibit the electron mobility of 0.22 cm^2 V^{-1} s^{-1} for **Hex-CO** and 7.5×10^{-3} cm^2 V^{-1} s^{-1} for **Hept-CO**. All these results suggest that the quinone unit can be used as the bridge to lower the molecular orbital energy levels, extend the molecular length, increase the molecular overlapping, and engineer the molecular stacking mode in the crystals. We believe that extending the length of azaacene derivatives through quinone bridges should be a promising way to achieve high-performance organic semiconductors in OFETs and other organic electronic devices.

Conflicts of interest

There are no conflicts to declare.

Acknowledgements

Q.Z. acknowledges financial support from AcRF Tier 1 (RG8/16, RG114/16), Singapore. This work was partially supported by JSPS KAKENHI Grant Numbers JP17H03042, JP16H02286 and JP26105004.

References

1 (a) M. Ganschow, S. Koser, S. Hahn, F. Rominger, J. Freudenberg, U. H. F. Bunz, *Chem.-Eur. J.* 2017, **23**, 4415; (b) L. Ji, M. Haehnel, I. Krummenacher, P. Biegger, F. L. Geyer, O. Tverskoy, M. Schaffroth, J. Han, A. Dreuw, T. B. Marder, U. H. F. Bunz, *Angew. Chem. Int. Ed.* 2016, **55**, 10498; (c) P.-Y. Gu, Y. Zhao, J.-H. He, J. Zhang, C. Wang, Q.-F. Xu, J.-M. Lu, X. W. Sun, Q. Zhang, *J. Org. Chem.* 2015, **80**, 3030; (d) J. Li, Q. Zhang, *ACS Appl. Mater. Interfaces*, 2015, **7**, 28049.

2 (a) P.-Y. Gu, F. Zhou, J. Gao, G. Li, C. Wang, Q.-F. Xu, Q. Zhang, J.-M. Lu, *J. Am. Chem. Soc.* 2013, **135**, 14086; (b) G. Li, K. Zheng, C. Wang, K. S. Leck, F. Hu, X. W. Sun, Q. Zhang, ACS Appl. Mater. Interface, 2013, **5**, 6458; (c) C. Wang, J. Wang, P. Li, J. Gao, S. Y. Tan, W. Xiong, B. Hu, P. S. Lee, Y. Zhao, Q. Zhang, *Chem Asian J.* 2014, **9**, 779; (d) C. Wang, P. Gu, B. Hu, Q. Zhang, *J. Mater. Chem. C,* 2015, **3**, 10055.

3 (a) P.-Y. Gu, Z. Wang, F.-X. Xiao, Z. Lin, R. Song, Q.-F. Xu, J.-M. Lu, B. Liu, Q. Zhang, *Mater. Chem. Front.* 2017, **1**, 495; (b) J. Li, S. Chen, Z. Wang, Q. Zhang, *Chem. Rec.,* 2016, **16**, 1518-1530

4 (a) V. Lami, D. Leibold, P. Fassl, Y. J. Hofstetter, D. Becker-Koch, P. Biegger, F. Paulus, P. E. Hopkinson, M. Adams, U. H. F. Bunz, S. Huettner, I. Howard, A. A. Bakulin, Y. Vaynzof, *Solar RRL* 2017, **1**, 1700053; (b) P.-Y. Gu, N. Wang, C. Wang, Y. Zhou, G. Long, M. Tian, W. Chen, X. W. Sun, M. G. Kanatzidis, Q. Zhang, *J. Mater. Chem. A* 2017, **5**, 7339; (c) N. Wang, K. Zhao, T. Ding, W. Liu, A. S. Ahmed, Z. Wang, M. Tian, X. W. Sun, Q. Zhang, *Adv. Energy Mater.* 2017, **7**, 1700522; (d) P.-Y. Gu, N. Wang, A. Wu, Z. Wang, M. Tian, Z. Fu, X. W. Sun, Q. Zhang, *Chem. Asian J.* 2016, **11**, 2135.

5 (a) F. Paulus, B. D. Lindner, Rei; F. Rominger, A. Leineweber, Y. Vaynzof, H. Sirringhaus, U. H. F. Bunz, *J. Mater. Chem. C*, 2015, **3**, 1604; (b) Q. Miao, *Adv. Mater.* 2014, **26**, 5541; c) X. Xu, Y. Yao, B. Shan, X. Gu, D. Liu, J. Liu, J. Xu, N. Zhao, W. Hu, Q. Miao, *Adv. Mater.* 2016, **28**, 5276.

6 (a) U. H. F. Bunz, *Acc. Chem. Res.* 2015, **48**, 1676; (b) A. H. Endres, M. Schaffroth, F. Paulus, H. Reiss, H. Wadepohl, F. Rominger, R. Krämer, U. H. F. Bunz, *J. Am. Chem. Soc.* 2016, **138**, 1792; c) B. Kohl, F. Rominger, M. Mastalerz, *Angew. Chem. Int. Ed.* 2015, **54**, 6051; (c) P.-Y. Gu, Z. Wang, G. Liu, H. Yao, Z. Wang, Y. Li, J. Zhu, S. Li, Q. Zhang, *Chem. Mater.* 2017, **29**, 4172; (d) L. Jiang, A. C. Papageorgiou, S. C. Oh, Ö. Sağlam, J. Reichert, D. A. Duncan, Y.-Q. Zhang, F. Klappenberger, Y. Guo, F. Allegretti, S. More, R. Bhosale, A. Mateo-Alonso, J. V. Barth, *ACS Nano* 2016, **10**, 1033.

7 (a) U. H. F. Bunz, J. U. Engelhart, B. D. Lindner, M. Schaffroth, *Angew. Chem. Int. Ed.* 2013, **52**, 3810; (b) U. H. F. Bunz, J. U. Engelhart, *Chem.-Eur. J.* 2016, **22**, 4680.

8 C. Wang, J. Zhang, G. Long, N. Aratani, H. Yamada, Y. Zhao, Q. Zhang, *Angew. Chem. Int. Ed.* 2015, **54**, 6292.

9 J. E. Anthony, *Chem. Rev.* 2006, **106**, 5028.

10 Z. Liang, Q. Tang, J. Xu, Q. Miao, *Adv. Mater.* 2011, **23**, 1535.

11 I. Kaur, W. Jia, R. P. Kopreski, S. Selvarasah, M. R. Dokmeci, C. Pramanik, N. E. McGruer, G. P. Miller, *J. Am. Chem. Soc.* 2008, **130**, 16274.

12 D. Matsumura, K. Kitazawa, S. Terai, T. Kochi, Y. Ie, M. Nitani, Y. Aso, F. Kakiuchi, *Org. Lett.* 2012, **14**, 3882.

13 Y.-Y. Liu, C.-L. Song, W.-J. Zeng, K.-G. Zhou, Z.-F. Shi, C.-B. Ma, F. Yang, H.-L. Zhang, X. Gong, *J. Am. Chem. Soc.* 2010, **132**, 16349.

14 D. Cortizo-Lacalle, C. Gozalvez, M. Olano, X. Sun, M. Melle-Franco, L. E. Hueso, A. Mateo-Alonso, *Org. Lett.* 2015, **17**, 5902.

15 J. U. Engelhart, F. Paulus, M. Schaffroth, V. Vasilenko, O. Tverskoy, F. Rominger, U. H. F. Bunz, *J. Org. Chem.* 2016, **81**, 1198.

16 B. D. Lindner, J. U. Engelhart, O. Tverskoy, A. L. Appleton, F. Rominger, A. Peters, H.-J. Himmel, U. H. F. Bunz, *Angew. Chem. Int. Ed.* 2011, **50**, 8588.

17 I. Pochorovski, C. Boudon, J.-P. Gisselbrecht, M.-O. Ebert, W. B. Schweizer, F. Diederich, *Angew. Chem. Int. Ed.* 2012, **51**, 262.

18 C. Wang, H. Dong, W. Hu, Y. Liu, D. Zhu, *Chem. Rev.* 2012, **112**, 2208.

19 Z. Wang, J. Miao, G. Long, P. Gu, J. Li, N. Aratani, H. Yamada, B. Liu, Q. Zhang, *Chem. Asian J.* 2016, **11**, 482.

20 M. Frisch, G. Trucks, H. Schlegel, G. Scuseria, M. Robb, J. Cheeseman, G. Scalmani, V. Barone, B. Mennucci, G. Petersson, *Inc., Wallingford, CT* **2009**.

21 H. Dong, X. Fu, J. Liu, Z. Wang, W. Hu, *Adv. Mater.* 2013, **25**, 6158.

22 Q. Tang, Y. Tong, H. Li, Z. Ji, L. Li, W. Hu, Y. Liu, D. Zhu, *Adv. Mater.* 2008, **20**, 1511.

23 (a) G. Schweicher, Y. Olivier, V. Lemaur, Y. H. Geerts, *Isr. J. Chem.* 2014, **54**, 595; (b) P. J. Skabara, J. B. Arlin, Y. H. Geerts, *Adv. Mater.* 2013, **25**, 1948.

24 (a) R. A. Marcus, *Rev. Mod. Phys.* 1993, **65**, 599; (b) J.-L. Brédas, D. Beljonne, V. Coropceanu, J. Cornil, *Chem. Rev.* 2004, **104**, 4971; (c) W.-Q. Deng, W. A. Goddard, *J. Phys. Chem. B* 2004, **108**, 8614.

25 X.-K. Chen, L.-Y. Zou, J.-X. Fan, S.-F. Zhang, A.-M. Ren, *Org. Electron.* 2012, **13**, 2832.

26 (a) E. F. Valeev, V. Coropceanu, D. A. da Silva Filho, S. Salman, J.-L. Brédas, *J. Am. Chem. Soc.* 2006, **128**, 9882; (b) A. Troisi, G. Orlandi, *J. Phys. Chem. B*, 2002, **106**, 2093.

View Article Online
DOI: 10.1039/C8TC00628H

A novel quinone bridged large azaacene exhibits electron mobility of 0.22 $cm^2 V^{-1} s^{-1}$ through molecular stacking structure engineering.